



Performance analysis of a double-pass solar air heater system with asymmetric channel flow passages

A. K. Raj¹ · G. Kunal¹ · M. Srinivas¹ · S. Jayaraj¹

Received: 1 June 2018 / Accepted: 21 September 2018 / Published online: 3 October 2018
© Akadémiai Kiadó, Budapest, Hungary 2018

Abstract

The present work seeks to address the forced convection heat transfer behaviour of a double-pass solar air heater system (DPSAHS) provided with asymmetric channel flow configuration used for solar drying of agro-products. Outdoor experiments were performed on a DPSAHS having a constant channel depth ratio of 1.5. Thermal response of the DPSAHS under different influencing parameters such as flow rate, channel depth, and thermophysical properties of the working fluid was experimentally determined. The influence of ambient parameters such as solar intensity, ambient temperature, wind speed, and relative humidity on the thermodynamic behaviour of the DPSAHS was also investigated. Among which, solar intensity and ambient temperature were found to be the major parameters influencing the energy and exergy efficiency followed by wind speed. Relative humidity was found to have the least percentage contribution towards the thermal characteristics of the system. Overall thermal efficiency and exergy efficiency were found to vary in the range of 20–41% and 5.6–18% at two different mass flow rates of 0.02 kg s⁻¹ and 0.03 kg s⁻¹, respectively. The results also inferred that the influence of thermophysical property variation on the thermodynamic performance depends upon the operating temperature range and on the nature of working fluid. Air temperature in the lower channel was found to be an average 3 °C higher than that of upper channel passage corresponding to two different mass flow rates. Hence, the thermodynamic behaviour of DPSAHS was found to be strongly influenced by the variation in channel depth, ambient parameters, and mass flow rate. The obtained experimental results were also compared with the available literatures.

Keywords Channel depth · Energy and exergy · Forced convection · Solar air heater

List of symbols

A	Area (m ²)	f	Friction factor
C_p	Specific heat (J kg ⁻¹ K ⁻¹)	G	Solar intensity (W m ⁻²)
D_c	Depth of channel passage (m)	h	Enthalpy (J kg ⁻¹) or heat transfer coefficient (W m ⁻² K ⁻¹)
D_h	Hydraulic diameter (m)	k	Thermal conductivity (W m ⁻¹ K ⁻¹)
\dot{E}	Energy (J)	K	Head-loss factor
\dot{E}_x	Exergy (J)	L	Length of the channel passage (m)
		\dot{m}	Mass flow rate (kg s ⁻¹)
		Nu	Nusselt number
		Δp	Pressure drop (N m ⁻²)
		Re	Reynolds number
		s	Entropy (J K ⁻¹)
		S_{gen}	Entropy generation (J K ⁻¹)
		T	Temperature (°C)
		U	Overall heat transfer coefficient (W m ⁻² K ⁻¹)
		V	Velocity (m s ⁻¹)
		W	Width of the channel passage (m)

✉ A. K. Raj
arunkraj03@gmail.com

G. Kunal
kunalgarud1@gmail.com

M. Srinivas
msrinivas@nitc.ac.in

S. Jayaraj
sjayaraj@nitc.ac.in

¹ Department of Mechanical Engineering, Solar Energy Centre, National Institute of Technology Calicut, NIT Campus P.O., Calicut, Kerala 673 601, India

Greek symbols

α Absorptivity

ϵ	Product of transmittance–absorptance
μ	Dynamic viscosity (Pa s)
ρ	Density (kg m^{-3})
σ	Stefan–Boltzmann constant
τ	Transmissivity
η	Efficiency

Subscripts

a	Ambient
avg	Average
b	Bottom plate
c	Collector
e	Edge
en	Entry
ext	Exit
f	Fluid
g	Glazing cover
ins	Insulation
p	Absorber plate
s	Sun or sides
w	Wind
I	Overall energy analysis
II	Exergy analysis

Introduction

Solar air heating systems are getting wide acceptance in domestic as well as commercial applications in the recent times. These systems are simple in design, cost-effective, flexible for design improvements and have reasonable good performance efficiency. Over the last many decades, several authors presented vast amount of literatures stating the advantageous of solar air heaters (SAH). Suzuki [1] discussed a general form of theoretically based exergy analysis rooting from the fundamentals concepts and applicable to solar air collector systems. Hossein et al. [2] developed an integrated mathematical model relating optical and thermal parameters to analyse the exergetic characteristics of a single-pass air heater system. The results concluded that the exergy analysis was superior to optimize the performance than conventional energy analysis. Hernandez et al. [3] developed two analytical models to evaluate the performance of a double-pass solar air heater system based on two flow configurations. Thermal performance of a double-pass parallel and counter-flow systems were analysed. Velmurugan and Kalaivanan [4] developed an analytical model to compute the energy and exergy efficiencies of a multi-pass solar air heater system. The obtained result agreed with the previous literature findings, and established the significance of provision of multi-pass

configurations to improve the overall efficiency of the air heater system.

Hollands and Shewen [5] analysed the effect of geometry of the flow channel passages on the overall heat transfer coefficient in solar air heating systems. The results inferred that, as the channel length becomes shorter (< 1 m), there was a maximum improvement in heat transfer coefficient. Verma et al. [6] developed a mathematical model to study the effect of channel depth and flow rate on different air heater configurations. The analysis revealed that double-pass air heater with single glazing cover yielded better performance. Mortazavi and Ameri [7] based on two configurations (conventional flat plate as well as one with a provision of a thin metal sheet) performed conventional as well as advanced exergetic analysis. The effect of parameters such as solar intensity, channel depth, and Reynolds number on the exergy annihilation was analysed. Gupta and Kaushik [8] presented a detailed performance and parametric investigation on a conventional flat plate solar air collector. The effect of optimum channel depth and aspect ratio of the solar collector on the maximum efficiency of the system was theoretically evaluated. The results concluded that the channel depth had a significant effect on the performance of solar collector system. An analytical formulation was developed to optimize the channel geometry of conventional solar air collectors by Hegazy [9]. Based on the results obtained, an optimum depth to length ratio (D/L) was proposed for flat plate SAH systems. Sun et al. [10] performed a CFD-based analysis to evaluate the performance of various configuration of SAH system with different channel depths. The obtained results concluded that the ratio of upper to lower channel depths in SAH should be a minimum value of one. Kalogirou et al. [11] presented a brief review on exergy analysis and its significance in performance evaluation and optimization of solar collectors in a wide variety of applications solar drying, energy storage, hybrid systems, power generation, etc.

The literature cited above states the conventional thermodynamic analysis performed over solar air heater systems based on analytical and numerical models. In the present work, an attempt was made to compute the energy and exergy of a double-pass solar air heater system using a fabricated novel experimental test facility comprising of asymmetric channel flow passages. Outdoor experiments were performed at NIT Calicut. The dependence on DPSAHS performance characteristics on the account of various influencing parameters was elaborately discussed. A detailed parametric study was also conducted to understand the effect of ambient conditions on the thermal behaviour of DPSAHS. Design modifications were also suggested for the fabricated DPSAHS for its overall

performance improvement, based on the obtained experimental results.

Experimental study

Geographical location

The south Indian peninsular state of Kerala lies in the tropical zone and the northern parts of this state receive a monthly average of $6.25 \text{ kWh m}^{-2} \text{ day}^{-1}$ of solar radiation, even during the winter months of November and December. An annual average of 2344 sunshine hours was recorded based on the previous year's data analysed. The experimental setup was installed at the Solar Energy Centre under the Department of Mechanical Engineering at NIT Calicut (latitude: 11.32°N , longitude: 75.93°E). The ambient temperature varied in the range of $22\text{--}34^\circ\text{C}$ and an average wind speed of 10 km h^{-1} was recorded at this location. A minimum of three experimental trials were carried out to ensure the accuracy of each of the obtained experimental results.

Test facility

A double-pass solar air heater system (DPSAHS) consists of a single glazing (transparent) cover made of 4 mm thick common glass cover, an absorber plate made of 1 mm thick copper sheet, a bottom plate made of 0.46 mm thick G.I. sheet and double-channel passages of distinct depths. The absorber and the bottom plate is painted black to ensure maximum absorption of the transmitted radiation from the glazing cover. It is to be noted that both surfaces are flat and no roughness geometries or fins are incorporated to enhance the thermal performance of the described system.

Figure 1 represents the schematic diagram of the experimental test system. A divergent section is provided at the upstream end of the upper channel passage (rectangular) to ensure the uniformity of flow throughout the system. In addition, a convergent section is provided at the downstream end of the passage to facilitate easier flow exit from the DPSAHS. Table 1 describes the geometrical configuration of the various components as described. A single inlet centrifugal air blower with 1H.P. capacity and 2800 rated rpm is used to drive the ambient air inside the DPSAHS. The air blower is then connected to the DPSAHS through an orifice meter, U-tube manometer and a manually operated gate valve. The pressure variation across the orifice is measured using a U-tube manometer. In order to control the mass flow rate of air into the DPSAHS, a manual gate valve is used. To ensure maximum solar incidence over the collector surface, a tilt angle of 10.18° with respect to horizontal [12] is provided to the

overall system and is installed facing south. All the three sides (namely, bottom, left and right surfaces) of the DPSAHS are thermally insulated using 50 mm thick polyurethane foam (PUF). Table 2 lists out the component-wise optical parameters of the overall system used for the present analysis.

Instrumentation

An air blower (1 H.P, 2800 rpm) is used to drive the ambient air through the solar air heater asymmetric channel passages. Mass flow rate is varied using a manually operated gate valve. A differential U-tube manometer with water as the manometric fluid connected at an optimum entrance length (upstream to the blower) is used to measure the variation in flow rate. In addition, the differential pressure measurements are computed with the help of a differential manometer provided at the inlet and outlet ends of the DPSAHS. The average value of coefficient of discharge (C_d) of the orifice meter after calibration is found to be 0.64.

Instantaneous solar radiation incident over the collector surface is recorded using an industrial standard pyranometer with a nominal accuracy of $\pm 5 \text{ W m}^{-2}$. The ambient temperature, wet bulb temperature, dew point temperature, and relative humidity are monitored and recorded using a weather station installed at the Solar Energy Centre of NIT Calicut. The nominal accuracy of the listed parameters in the weather station is $\pm 0.5^\circ\text{C}$ for temperatures and $\pm 3\%$ for relative humidity. The ambient wind speed is measured using a cup-type anemometer integrated within the weather station. The nominal accuracy of the anemometer is in the range of $\pm 1 \text{ m s}^{-1}$. Temperature sensors (K-type thermocouples) with an accuracy of $\pm 0.5^\circ\text{C}$ are positioned at eighteen different locations within the DPSAHS, as shown in Fig. 2. The outlet velocity of the air mass from the DPSAHS is also measured with a vane-type anemometer having a nominal accuracy of $\pm 0.01 \text{ m s}^{-1}$. All the measurements are frequently monitored and recorded every minute in the computer database using a data logging system (Envada, 16-channel data logger).

Experimental procedure

A major challenge faced during the design and fabrication of the described DPSAHS was to obtain a leak-proof working model for carrying out the present analysis. Using simple conventional methods, a leak test was performed and the constructed model was found to be satisfactory to carry out the present experimental analysis. Experiments were carried out during the months of November and December 2017. The obtained data were used to compute

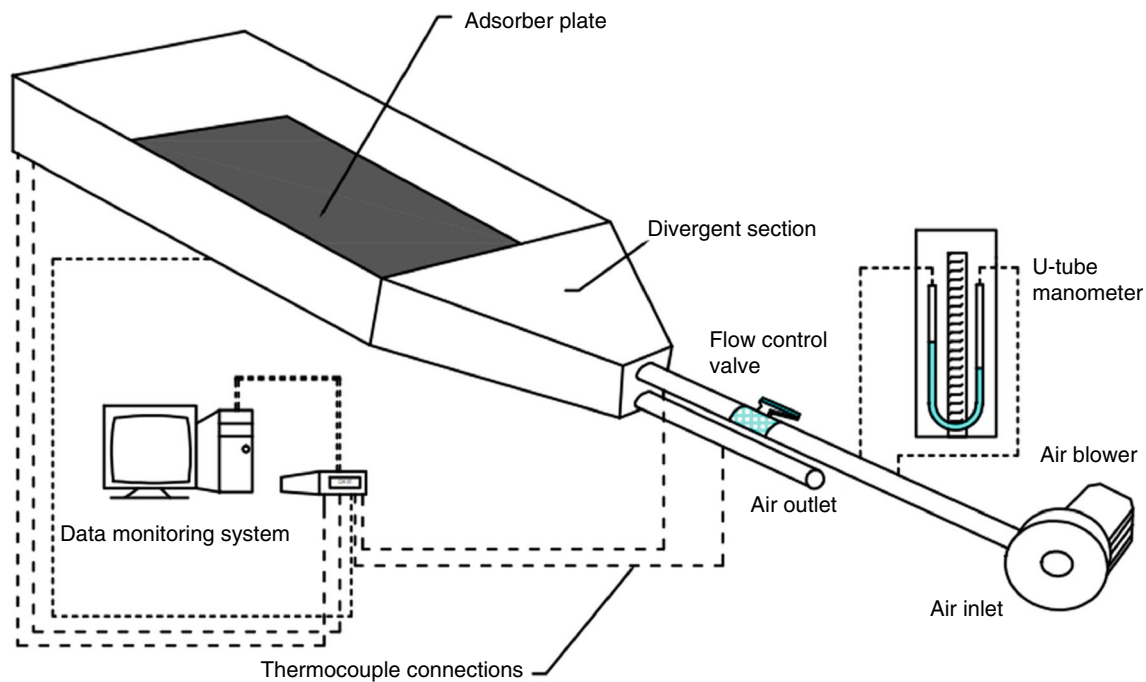


Fig. 1 Schematic representation of experimental setup

Table 1 Description of the geometrical features of various components

Parameter	Dimensions/mm
Glazing cover	1380 × 650 × 4
Absorber plate	1250 × 670 × 1
Bottom plate	1500 × 670 × 0.46
Upper channel passage	1500 × 670 × 150
Lower channel passage	1500 × 670 × 100

Table 2 Optical properties of various components of the test facility [7]

Optical parameters	Values
Emissivity of glass, ε_g	0.88
Emissivity of absorber, ε_p	0.95
Emissivity of bottom plate, ε_b	0.95
Absorptivity of absorber surface, α_p	0.95
Transmissivity of glazing cover, τ_g	0.92

the thermodynamic efficiencies (η_I and η_{II}) of the DPSAH test facility. The experiments performed within the DPSAHS were entirely based on the test standards suggested by ASHRAE [13]. The experimental investigation was performed corresponding to two different mass flow rates of 0.02 kg s^{-1} and 0.03 kg s^{-1} , respectively. For

each variation in flow rate, the experiments were performed consecutively, until a minimum of 3 days with reliable ambient environmental conditions was obtained. Among which, 2 days of experimental data (6th December, 2018 and 8th December, 2018) with reliable meteorological conditions (mainly, solar intensity, ambient temperature, wind speed and relative humidity) was selected for comparison, corresponding to both flow rates. All the measurements are monitored and recorded as explained in Sect. 2.3. The experiments were started from 7:00 am and continued up to 17:00 pm (IST). However, the data recorded between 8:00 am to 17:00 pm were used for the present analysis. A one-hour time gap was initially provided to allow the preheating of various components enclosed within the overall DPSAHS.

Uncertainty analysis

In order to assure the accuracy of the obtained results from the experiments performed on the DPSAHS, an uncertainty analysis was carried out. The deviation of the measured data from the true value can be either due to the sensitivity of the measuring equipment is used or may be due to the measurement errors. Detailed descriptions of nominal accuracies of various instruments are reported in Sect. 2.3. The factors which influence the performance of the overall system includes solar intensity, ambient temperature, wind speed, mass flow rate and the temperature gained by the air mass. Based on a linearized fractional

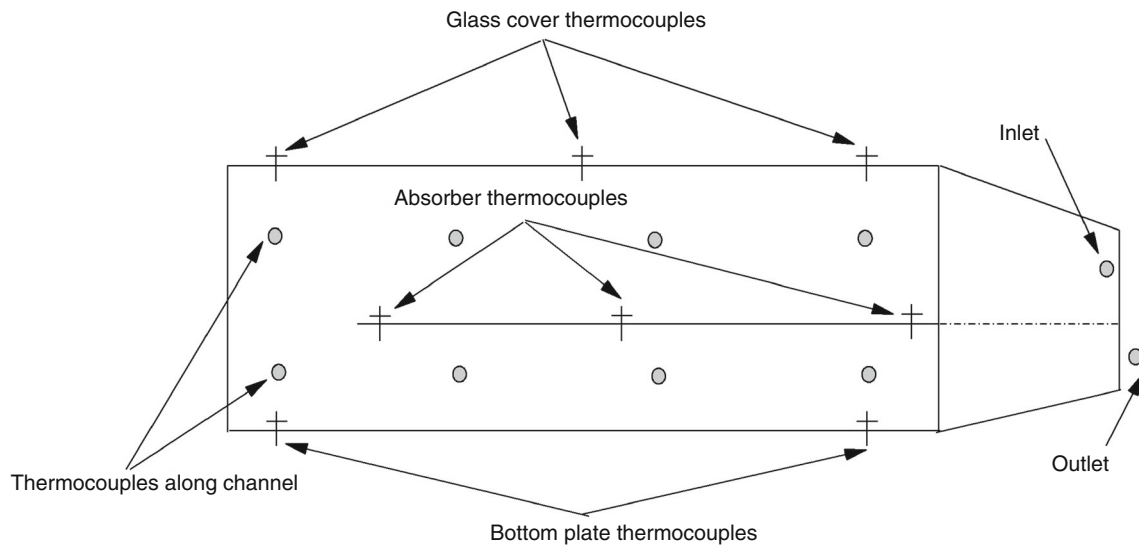


Fig. 2 Location of temperature sensors within the DPSAHS

approximation, the uncertainties associated with air flow rate, energy gained, overall efficiency and exergy efficiency are calculated using the following Eqs. (1)–(4) as described.

$$\frac{w_{\dot{m}}}{\dot{m}} = \sqrt{\left(\frac{w_{V_{avg}}}{V_{avg}}\right)^2 + \left(\frac{w_{T_a}}{T_a}\right)^2 + \left(\frac{w_{P_a}}{P_a}\right)^2} \tag{1}$$

$$\frac{w_Q}{Q} = \sqrt{\left(\frac{w_{\dot{m}}}{\dot{m}}\right)^2 + \left(\frac{w_{T_{in}}}{T_{in}}\right)^2 + \left(\frac{w_{T_{out}}}{T_{out}}\right)^2} \tag{2}$$

$$\frac{w_{\eta_I}}{\eta_I} = \sqrt{\left(\frac{w_{\dot{m}}}{\dot{m}}\right)^2 + \left(\frac{w_{\Delta T}}{\Delta T}\right)^2 + \left(\frac{w_G}{G}\right)^2} \tag{3}$$

$$\frac{w_{\eta_{II}}}{\eta_{II}} = \sqrt{\left(\frac{w_{\dot{m}}}{\dot{m}}\right)^2 + \left(\frac{w_{T_{in}}}{T_{in}}\right)^2 + \left(\frac{w_{T_{out}}}{T_{out}}\right)^2 + \left(\frac{w_{T_a}}{T_a}\right)^2 + \left(\frac{w_{\Delta p}}{\Delta p}\right)^2 + \left(\frac{w_G}{G}\right)^2} \tag{4}$$

It can be noted that the factors influencing both energy and exergy efficiencies are obtained based on Eqs. (41) and (52), given in Sect. 4. The results obtained indicate that the uncertainties associated with temperature, air mass flow rate, overall and exergy efficiencies were 0.0215, 0.0376, 0.0762, and 0.0842, respectively. Table 3 describes the

Table 3 Uncertainties associated with output parameters

Parameters	Range	Uncertainty/%
Temperatures (T_{in} and T_{out})	28–51	± 2.15
Mass flow rate	0.015–0.03	± 3.76
Overall efficiency	20–41	± 7.62
Exergy efficiency	5–18	± 8.42

operating range and the corresponding uncertainties attributed with each parameter.

Modelling of solar air heaters

In the present analysis, it is mandatory to understand the effect of ambient parameters such as ambient temperature, solar intensity, wind speed, and relative humidity on the overall thermodynamic characteristics of DPSAHS. Parametric response of the system due to variation in these ambient environmental conditions is studied using tools such as artificial neural network (ANN) and analysis of variance (ANOVA). A detailed description of these techniques is provided in this section.

Artificial neural network (ANN)

ANN tool makes use of experimental observations to formulate prediction models by adopting training and learning strategy. Thermal responses of the DPSAHS such as overall thermal efficiency and exergy efficiency were found to be affected by ambient factors such as solar intensity, ambient temperature, wind speed and relative humidity. These ambient factors were chosen as the input network parameters whereas the thermal efficiency and the exergy efficiency were considered to be the output (response) parameters. Experiments were conducted during the selected period of 25 days in the months of November and December in 2017. To train the ANN network, four hundred and sixty-four data sets obtained per day from the experiments were utilized. The predicted values were then compared with the experimental observations obtained

under clear sky conditions (06.12.2017 and 08.12.2017) to test the accuracy of the developed ANN model network.

A feed-forward back propagation (FFBP) algorithm is the most widely used ANN algorithm for modelling of solar air heater system [14–16]. Hence, FFBP algorithm with 25 hidden neurons in the hidden layer, four neurons in the input layer and two neurons in the output layer was used for the present analysis. Figure 3 shows the ANN network architecture used for the present analysis. The number of hidden neurons is optimized using Eq. (5) [17].

Number of hidden neurons

$$= 0.5(\text{input neurons} + \text{output neurons}) + \sqrt{\text{No of training data}} \quad (5)$$

For the present experimental analysis, ANN tool was only used to obtain the required outputs to perform the ANOVA analysis. ANN modelling was performed in MATLAB[®] using NN toolbox. Several combinations of training variants namely, LM (Lavenberg–Marguardt), SCG (Scaled Conjugate Gradient) and CGP (Conjugate Gradient Pola–Ribiere) along with activation functions such as Log-Sigmoidal and Tan-Sigmoidal were used for developing different ANN models. On the basis of the statistical parameters such as coefficient of determination (R^2), root mean square error (RMSE) and coefficient of variance (COV), it was found that FFBP algorithm with LM and Log-Sigmoidal as the activation function yielded accurate results when compared to the experimental observations. In general, the values of the statistical parameters can be computed using Eqs. (6–8) as shown. Hence, an optimized ANN model with network architecture (4-25-2) was used for carrying out the present analysis.

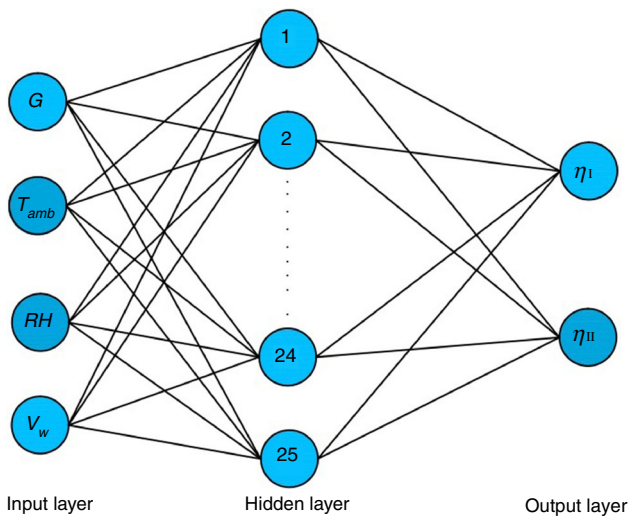


Fig. 3 ANN architecture used for the present analysis

$$R^2 = 1 - \frac{\sum_{i=1}^n (\text{Exp}_v - \text{ANN}_v)^2}{\sum_{i=1}^n (\text{Exp}_v)^2} \quad (6)$$

$$\text{RMSE} = \sqrt{\frac{1}{n} \sum_{i=1}^n (\text{Exp}_v - \text{ANN}_v)^2} \quad (7)$$

$$\text{COV} = \frac{\text{RMSE}}{\frac{1}{n} \sum_{i=1}^n \text{Exp}_v} \quad (8)$$

Analysis of variance (ANOVA)

The most significant ambient parameter that strongly influences the thermodynamic behaviour of the DPSAHS was investigated using analysis of variance (ANOVA) technique. Overall thermal efficiency and exergy efficiency were considered to be the major thermal characteristics of the system. A prediction model developed using ANN tool was used to perform the analysis in ANOVA. As mentioned, four ambient parameters namely, solar intensity, ambient temperature, wind speed and relative humidity was selected for the analysis. The operating ranges of these corresponding ambient parameters are listed in Table 4. Based on the adopted three-level design principle, a total of 81 (3^4) factorial designs comprising of different combinations of input parameters were obtained. Table 5 describes the various combinations of input parameters grouped into three different levels. Accordingly, each input parameter was sub-divided into three levels, namely, low, medium and high. To perform the analysis using ANOVA, the required minimum number of input data sets can be computed using Eq. (9) as described.

$$N_d = 1 + n_p(L - 1) \quad (9)$$

Here, N_d represents the total number of input data sets required, n_p stands for the number of influencing parameters used and L accounts for the number of level used for computation. A minimum of nine input data sets are required to carry out the present analysis based on Eq. (9). The output values corresponding to these nine combinations of the input data sets were obtained using the developed ANN model. A generalized linear model was then used to find out the relative percentage contribution of various input parameters on the overall thermal efficiency and exergy efficiency of the DPSAHS. Equations (10–16) are used to determine the percentage contribution of each of the input parameter on the thermal behaviour of the system [17].

The degree of freedom (DOF) of each input ambient parameter is calculated as:

$$\text{DOF} = L - 1 \quad (10)$$

The mean sum of squares (MSS) is evaluated by

Table 4 Ambient parameters and various levels used for ANOVA analysis

Parameters	Solar intensity	Ambient temperature	Wind velocity	Relative humidity
Level-1	100	24	0.5	50
Level-2	410	28	2.5	60
Level-3	720	32	4.5	70

Table 5 Percentage contribution of different ambient parameters on thermal performance

Source	Degrees of freedom	Sum of squares	Mean sum of squares	Pure sum of squares	Percentage contribution
η_I					
Solar intensity	2	125.08	62.5405	125.079	44.52
Ambient temperature	2	137.94	68.968	137.936	49.09
Wind speed	2	11.414	5.707	11.414	4.06
Relative humidity	2	6.522	3.261	5.522	2.32
Error	0				0
Total	8	280.954			100.0
η_{II}					
Solar intensity	2	128.08	64.038	128.076	50.09
Ambient temperature	2	103.85	51.9235	103.847	40.61
Wind speed	2	15.94	7.968	15.936	6.23
Relative humidity	2	7.83	3.913	7.826	3.06
Error	0				0
Total	8	255.685			100.0

$$MSS = \frac{SS}{DOF} \quad (11)$$

Pure sum of squares (PSS) is evaluated using the relation

$$PSS = MSS - MSS_{PE} \times DOF \quad (12)$$

The percentage contribution (PC) is given by

$$PC = \frac{PSS}{TSS} \quad (13)$$

Here, SS denotes the sum of squares corresponding to each input parameter and is stated using the relation

$$SS = \left(L \times \sum_{i=1}^L \bar{P}_{Li}^2 \right) - SS_M \quad (14)$$

Here P_{Li} stands for the input parameter at different levels considered for analysis. The sum of squares due to mean (SS_M) is given as

$$SS_M = N_d \times SS_{avg} \quad (15)$$

and

The total sum of squares is given by

$$TSS = \sum_{i=1}^{n_p} SS_i \quad (16)$$

Energy and exergy analysis

Energy

First law of thermodynamics was widely used over several decades to evaluate the thermal performance characteristics of energy systems. In general, when the input energy is derived from intermittent renewable energy sources such as solar energy, the thermal performance of the system is commonly evaluated based on instantaneous (η) and overall efficiency (η_I). The interaction of various components such as glazing cover, absorber surface, bottom plate, and working fluid (air) flowing through the channel passages, and taking part in energy exchange can be evaluated based on energy balance principles. To compute the effect of each of these parameters, optical properties of glazing cover and absorber surface, solar intensity, collector area, flow rate, surface temperatures, and thermophysical properties of working fluid should be well defined. The various assumptions considered for the present analysis are:

- Conduction resistance associated with absorber, bottom plate, and glazing cover is neglected

- The temperatures of absorber and bottom plate surfaces are assumed to be uniform
- The temperature gradient within the glass cover is assumed to be negligible
- Convective heat transfer coefficient between air, absorber, and bottom plate is assumed to be identical
- Energy losses along the edges of the DPSAHS is neglected
- There is no energy interaction between the system and surroundings.

Based on the first law of thermodynamics, Eq. (17) represents the energy interaction [18] expressed as:

$$\dot{E}_{AB} = \dot{E}_U + \dot{E}_{AC} + \dot{E}_L \quad (17)$$

where \dot{E}_{AB} is the energy absorbed, \dot{E}_U defines the useful energy extracted, \dot{E}_{AC} stands for the energy accumulation and \dot{E}_L corresponds to the energy lost to the surroundings. The amount of energy absorbed by the absorber surface from the incident radiation on the glazing cover is a function of optical product (transmittance-absorptance factor), and is evaluated using Eq. (18) as

$$\dot{E}_{AB} = \epsilon GA_p \quad (18)$$

where ϵ represents the factor of the product of transmittance-absorptance ($\epsilon = \alpha_p \tau_g$).

The amount of useful energy extracted by the working fluid from the system is calculated using Eq. (19).

$$\dot{E}_U = \dot{m} C_p (T_{out} - T_{in}) \quad (19)$$

In general, the energy accumulation term is often used when the system is incorporated with sensible or latent heat thermal storage materials such as rock, water, paraffin wax, salts, etc. In the present work, as there is no inclusion of energy storage materials, the energy accumulation term is neglected. However, the energy lost to the surrounding environment is accounted using Eq. (20), which is represented as:

$$\dot{E}_L = U_L A_b (T_b - T_a) \quad (20)$$

where the overall energy loss coefficient (U_L) is the sum total of energy lost from the glazing cover (U_g), bottom plate (U_b) and through the edges (U_s) of the enclosure. The terms thus described comprises of convection and radiation heat transfer coefficients, which can be estimated from their fundamental definitions using Eqs. (21) to (25) and Eq. (30).

$$U_g = \left[\left[\frac{1}{h_{c(p-g)} + h_{r(p-g)}} \right] + \left[\frac{1}{h_{c(g-a)} + h_{r(g-a)}} \right] \right]^{-1} \quad (21)$$

Here, the general formula representation of radiative heat transfer coefficient between two parallel plates is

$$h_{r(s_1-s_2)} = \left[\frac{\sigma (T_{s_1}^2 + T_{s_2}^2) (T_{s_1} + T_{s_2})}{\left(\frac{1}{\epsilon_{s_1}} \right) + \left(\frac{1}{\epsilon_{s_2}} \right) - 1} \right] \quad (22)$$

The convective heat transfer coefficient between the glazing cover and the ambient environment is given by McAdams correlation [19], given as

$$h_{c(g-a)} = 5.67 + 3.86 V_w \quad (23)$$

The radiative heat transfer coefficient between the glazing cover is expressed as

$$h_{r(g-a)} = \epsilon_g \sigma (T_g^2 + T_{sky}^2) (T_g + T_{sky}) \quad (24)$$

where T_{sky} , which can be estimated using Swinbank correlation given in the form [20]

$$T_{sky} = 0.0552 T_a^{1.5} \quad (25)$$

The convective heat transfer coefficient between the air, absorber surface and the bottom plate surface is computed using the correlation for average Nusselt number [19] as stated in Eqs. (26) to (28), respectively.

$$Nu_{avg} = 4.9 + \frac{0.0606 (Re Pr D_h / L)^{1.2}}{1 + 0.0909 (Re Pr D_h / L)^{0.7} Pr^{0.17}} \quad (26)$$

where Re is the Reynolds number and is computed as

$$Re = \frac{\rho V_{avg} D_h}{\mu} \quad (27)$$

The hydraulic diameter appearing in Eq. (26) can be obtained from the expression

$$D_h = \frac{2WD_c}{W + D_c} \quad (28)$$

In Eq. (29), D_r is the ratio of upper channel depth (D_{c_up}) to lower channel depth (D_{c_lc}) of the DPSAHS passage.

$$\text{i.e., } D_r = \frac{D_{c_up}}{D_{c_lc}} \quad (29)$$

For the fabricated DPSAHS, the channel depth ratio (D_r) is fixed as 1.5. The convective heat transfer coefficient is obtained using the relation

$$h_{c(p-f)} = h_{c(b-f)} = \frac{Nu k_f}{D_h} \quad (30)$$

The thermophysical property variations of the working fluid with respect to the operating conditions are obtained employing the following correlations [7] stated as in Eqs. (31)–(33), respectively.

$$k_f = (0.0015215 + 0.097459T_f - 3.3322 \times 10^{-5}T_f^2) \times 10^{-3} \tag{31}$$

$$\rho_f = 3.9147 - 0.016082T_f + 2.9013 \times 10^{-5}T_f^2 - 1.9407 \times 10^{-8}T_f^3 \tag{32}$$

$$\mu_f = (1.6157 + 0.06523T_f - 3.0297 \times 10^{-5}T_f^2) \times 10^{-6} \tag{33}$$

It must be noted that the working fluid temperature changes as it flows through the upper and lower channel passages, as there is variation in flow channel depths. Hence, for simplicity, an average temperature of the working fluid (separately for upper and lower channels) is used to estimate the thermophysical property variation. The energy loss coefficient through the bottom plate as well as the edge loss coefficient is calculated using Eqs. (34) and (35).

$$U_b = \frac{k_{ins}}{\Delta x_{ins}} \tag{34}$$

$$U_s = \frac{(L_c + W_c)D_c k_{ins}}{L_c W_c L_e} \tag{35}$$

In addition, the channel pressure drop (Δp_c), the inlet and exit pressure drop (Δp_E) within the DPSAHS is calculated using the following Eqs. (36)–(39) as described.

$$\Delta p_c = 2 \frac{f \rho_f L V_{avg}^2}{D_h} \tag{36}$$

The friction factor (f) for turbulent flow [21] appearing in Eq. (36) is calculated using the following expression

$$f = 0.0791 Re^{-0.25} \text{ (valid for } Re > 2300) \tag{37}$$

$$\Delta p_E = \frac{K \rho_f V_{avg}^2}{2} \tag{38}$$

where K denotes the head-loss factor and is estimated from

$$K = \frac{0.5 \left(1 - \frac{D_{h0}}{D_h}\right)}{\left(\frac{D_{h0}}{D_h}\right)^4} \tag{39}$$

The instantaneous thermal efficiency and the daily overall efficiency of the DPSAHS are calculated by the stated expressions in Eqs. (40) and (41).

$$\eta = \frac{\dot{m} C_p \Delta T}{G A_c} \tag{40}$$

$$\eta_I = \frac{\int \dot{m} C_p \Delta T}{\int G A_c} \tag{41}$$

In Eqs. (40) and (41) ΔT represents the temperature gained by air mass, G denotes the instantaneous solar intensity, A_c is the collector surface area and C_p is the specific heat capacity of air.

Exergy

The concept of exergy balance rooted from the fundamentals of thermodynamic principles, describes it as the useful work obtainable from a thermal system. The inference obtained from the exergy balance was found to be critical to optimize the overall system performance [22]. In this analysis, an attempt is made to calculate the exergy efficiency from the obtained experimental data. The commonly used assumptions in the present analysis are listed as follows [23–25]:

- Time-independent flow considerations
- Working fluid is assumed to be ideal with constant thermophysical properties
- Potential and kinetic energy effects are negligible
- Chemical and nuclear interactions are neglected
- Energy flowing into the system and work done by the system are considered to be positive

Based on these assumptions, Eq. (42) represents the general exergy balance equation [7] in the form:

$$\sum \dot{E}x_{in} - \sum \dot{E}x_{out} = \sum \dot{E}x_{dest} \tag{42}$$

(Or)

$$\sum \dot{E}x_{net,mass} + \sum \dot{E}x_{net,heat} - \sum \dot{E}x_{net,work} = \sum \dot{E}x_{dest} \tag{43}$$

Eqn (43) can be expanded by substituting for each individual term as shown in Eq. (44).

$$\sum \dot{m}_{in} \Psi_{in} - \sum \dot{m}_{out} \Psi_{out} + \sum \left(1 - \frac{T_a}{T_s}\right) \dot{Q}_s - \dot{W} = \dot{E}x_{dest} \tag{44}$$

where Ψ_{in} and Ψ_{out} are calculated by using Eqs. (45) and (46), respectively.

$$\Psi_{in} = (h_{en} - h_a) - T_a (s_{en} - s_a) \tag{45}$$

$$\Psi_{out} = (h_{ext} - h_a) - T_a (s_{ext} - s_a) \tag{46}$$

On substituting Eqs. (45) and (46) in Eq. (44), the resulting equation is described as Eq. (47).

$$\left(1 - \frac{T_a}{T_s}\right) \dot{Q}_s - \dot{m} [(h_{ext} - h_{en}) - T_a (s_{ext} - s_{en})] = \dot{E}x_{dest} \tag{47}$$

Here \dot{Q}_s represents the energy absorbed by the absorber surface. The value of \dot{Q}_s is evaluated using the relation given by Eq. (48).

$$\dot{Q}_s = G\alpha_p\tau_g A_c \quad (48)$$

Equations (49) and (50) are used to compute the corresponding enthalpy and entropy changes of air within the DPASHS. The obtained values of enthalpy and entropy are substituted back in Eq. (47).

$$\Delta h = h_{\text{ext}} - h_{\text{en}} = C_{p,\text{air}}(T_{f,\text{air}} - T_{i,\text{air}}) \quad (49)$$

$$\Delta s = s_{\text{ext}} - s_{\text{en}} = C_{p,\text{air}} \ln \frac{T_{f,\text{air}}}{T_{i,\text{air}}} - R \frac{P_{\text{ext}}}{P_{\text{en}}} \quad (50)$$

Altogether, Eqs. (48)–(50) represent each individual terms in the LHS of Eq. (47). The exergy destruction term on the RHS of Eq. (47) is then calculated using Eq. (51) and is expressed as:

$$\dot{E}x_{\text{dest}} = T_a S_{\text{gen}} \quad (51)$$

Based on the formulated equations, the overall exergy efficiency of the DPASHS is evaluated. It must be noted that the exergy destruction is only accounted during this analysis. No attempts were made to account for the exergy losses within the overall system. Net exergy efficiency is calculated as the ratio of net exergy out to the net exergy input to the overall system. Exergy efficiency is mathematically expressed using Eq. (52). The exergy leaving the system and exergy entering the overall DPASHS is calculated using the stated expression in Eqs. (53) and (54), respectively.

$$\eta_{II} = \frac{\dot{E}x_{\text{ext}}}{\dot{E}x_{\text{en}}} \quad (52)$$

where

$$\dot{E}x_{\text{ext}} = \dot{m}[(h_{\text{ext}} - h_{\text{en}}) - T_a(s_{\text{ext}} - s_{\text{en}})] \quad (53)$$

$$\dot{E}x_{\text{en}} = \left(1 - \frac{T_a}{T_s}\right) \dot{Q}_s \quad (54)$$

Results and discussion

Meteorological conditions

In this work, the required data used for the thermodynamic calculations were recorded during the winter months of November and December 2017. The incident solar radiation varied in the range of 100–720 W m⁻² with an average value of 410 W m⁻² during these months. These described values were based on the pattern of incident solar radiation received at the present location (11°32'N,

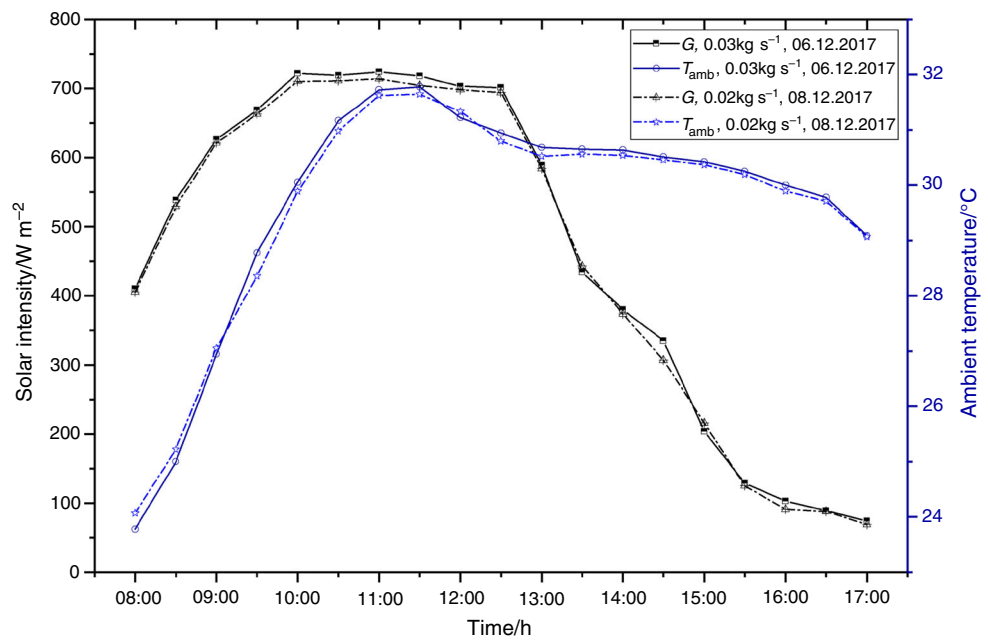
75°93'E). In general, the peak solar intensity was recorded between 11:00 am to 12:00 pm (IST) corresponding to the days in which experiments were performed. Even though, the experiments were carried out for a total time span of 9 h/day, the potential sunshine hours favourable for performing the experimentation were limited to 7 h/day. Figure 4 shows the variation of incident solar radiation and ambient temperature corresponding to two different days of experimental analysis. Ambient temperature and wind speed variations were monitored at every instance to understand the effect of heat gained by the air and to quantify the convection heat losses occurring from the DPASHS. The ambient temperature varied in the range of 24–32 °C as shown in Fig. 4. Similarly, the wind speed varied in the range of 0.5–4.5 m s⁻¹.

Temperature Gain (ΔT)

A mass flow rate of 0.02 kg s⁻¹ (experiment performed on 08.12.17) was maintained constant throughout the day for carrying out the experimental analysis. During the experiment, the ambient temperature was found to vary from 24.1 to 32 °C with a mean temperature of 28 °C. The recorded peak value of temperature for the absorber surface and the bottom plate was 68.4 °C and 56.2 °C, respectively. The maximum temperature gained by the air mass was observed to be 14.3 °C. The same experiment was repeated at a mass flow rate of 0.03 kg s⁻¹ (experiment performed on 06.12.17). The recorded data results obtained inferred that the peak absorber temperature and the maximum temperature gained by the air were 70.6 °C and 10.6 °C, respectively.

In principle, mass flow rate directly quantifies the nature of energy interaction taking place between the working fluid (air) and the enclosed surfaces within the DPASHS. At higher mass flow rate, the temperature gained by the air at any instant was found to be much lower than that at reduced mass flow rate. As flow rate increases, more volume of air interacts with the enclosed surfaces of the DPASHS. Thereby, the air extracts more amount of energy at each instance from the overall system. As a result, the temperature gained by the absorber surface, bottom plate as well as the glazing cover was continuously extracted out from the overall system by the flowing air. Similarly, the variation in absorber surface temperature corresponding to 0.03 kg s⁻¹ was found to be higher than that at 0.02 kg s⁻¹. At lower mass flow rate, the energy interaction between the air and the absorber surface at an instant prolongs for an extended duration. Therefore, at each instant, the magnitude of temperature gained by air through convection from the absorber surface was higher, which resulted in the lower values of absorber temperature.

Fig. 4 Solar intensity variation during 06.12.2017 and 08.12.2017



Channel depth

The experimental test system comprises of a double-pass configuration in which the channels are provided with different depths as described in Table 1. The upper channel passage between the absorber surface and the glass cover as well as the lower channel passage between the absorber surface and the bottom plate was provided with channel depth of 0.15 m and 0.1 m, respectively. Hence, there is a notable difference of 0.05 m in channel depth between the two channel passages of the DPSAHS. It was observed from the recorded data that the air temperature was greatly influenced by the variation of channel depths. At a mass flow rate of 0.02 kg s^{-1} , the maximum value of air temperature obtained was $51.8 \text{ }^{\circ}\text{C}$ and $55.1 \text{ }^{\circ}\text{C}$ for the upper and lower channel passages, respectively. As the solar intensity increases, the temperature gained by the absorber surface and the bottom plate increases. Therefore, the heat gained by the air increases, due to increase in temperature gradient by convection heat transfer. Similarly, the peak temperature value obtained for the upper and lower channel passages corresponding to a mass flow rate of 0.03 kg s^{-1} was $50.7 \text{ }^{\circ}\text{C}$ and $54.03 \text{ }^{\circ}\text{C}$, respectively. From the obtained results, it was concluded that, as the channel depth increases, the convective heat transfer between the air and the enclosed surfaces increases. Therefore, the temperature gained by the air increases. In other words, as the depth of channel passages increases, the temperature gained by the air from the enclosing surfaces decreases. Figure 5 shows the variation of air temperature along the upper and lower channel passages corresponding to two different mass flow rates.

The daily overall thermal efficiency and the exergy efficiency were found to be adversely affected by the variation in channel depth. As the flow proceeds through the channels with larger depths, the temperature gained by the air reduces. Therefore, the overall thermal efficiency of the system tends to decrease. Similarly, the exergy destruction was found to increase with respect to channel depth. As channel becomes deeper, interaction between the air and the enclosed surfaces of DPSAHS reduces. Hence, the absorber surface temperature, glass cover temperature and the bottom plate temperature tends to increase with increase in solar intensity. As the temperature builds up inside the DPSAHS, the net radiation heat transfer coefficient from these respective surfaces increases facilitating more heat losses. Thereby, the overall thermal performance characteristics of the DPSAHS reduce. These obtained results were found to be in good agreement with the reported findings of Mortazavi and Ameri [7], Sun et al. [9] and Forsen et al. [27].

Heat transfer coefficients

Radiation and convection heat transfer coefficients are computed using the relations stated in Sect. 4.1. Figure 6 shows these variations of radiation heat transfer coefficients taking part in the heat exchange between the absorber surface, bottom plate, and the surrounding environment at two different mass flow rates. The results obtained inferred that the radiation heat transfer coefficient was found to be higher in magnitude corresponding to the lower mass flow rate. It was possibly due to the continuous energy build up taking place at every instant inside the

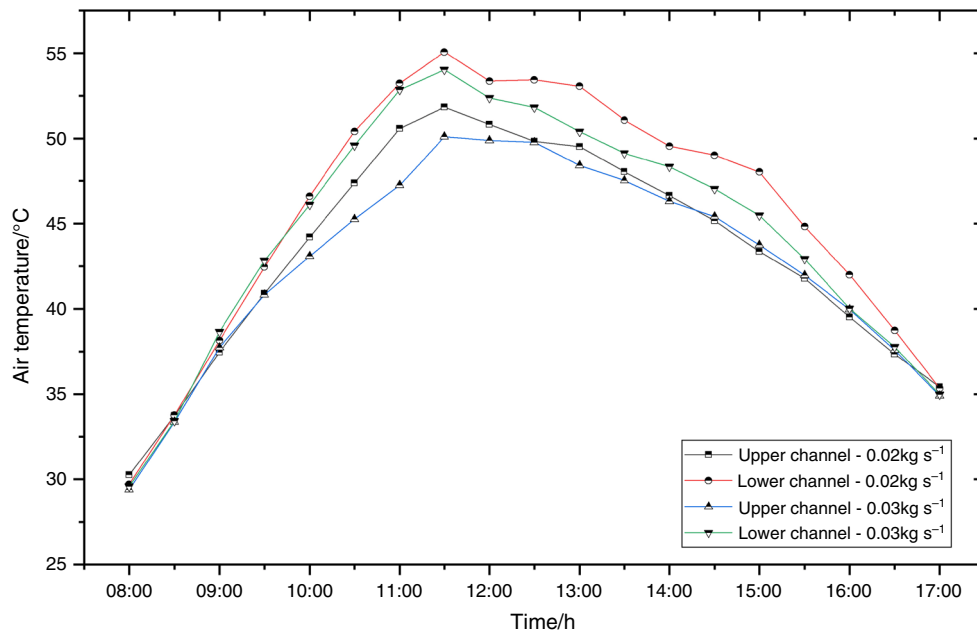
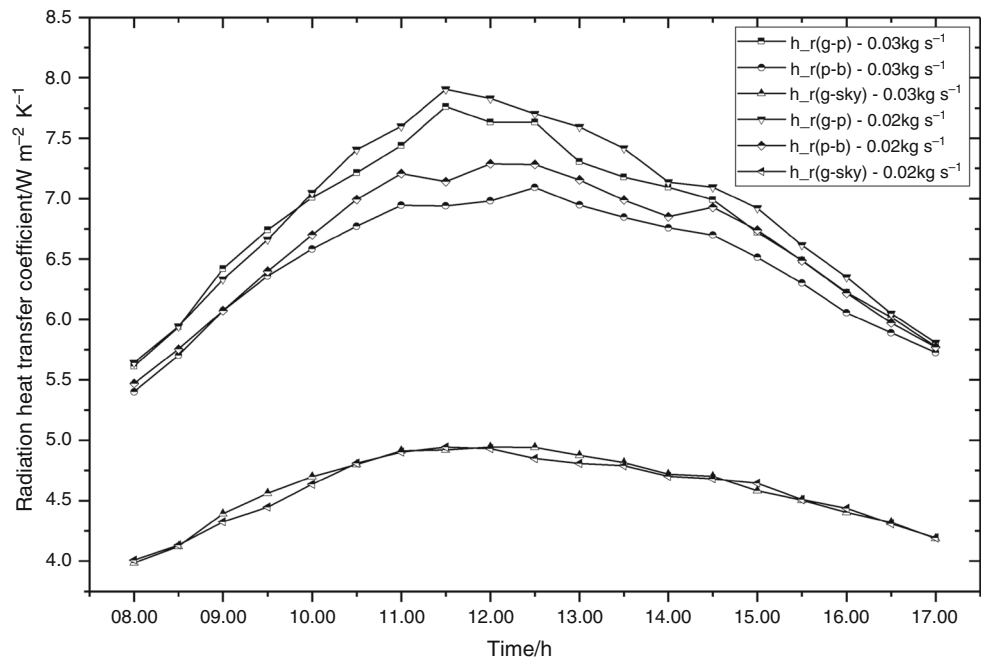


Fig. 5 Temperature gained by the air flowing through the upper and lower channels

Fig. 6 Comparison of radiation heat transfer coefficients corresponding to two different mass flow rates



enclosed surfaces of the DPSAHS corresponding to lower mass flow rate. On the other hand, the forced convection heat transfer coefficient was found to be higher at higher mass flow rate. In addition, it was observed that the convection heat transfer coefficient was marginally higher in magnitude for the lower channel when compared to that of the upper channel passage. It was solely due to more energy interaction occurring between the air and the enclosed surfaces of the DPSAHS leading to the temperature rise, as the air flows from the upper channel to the

lower channel passages. At a mass flow rate of 0.03 kg s^{-1} , the value of average heat transfer coefficient obtained was $10.6 \text{ W m}^{-2} \text{ K}^{-1}$ and $10.8 \text{ W m}^{-2} \text{ K}^{-1}$ for the upper and lower channel passages. Similarly, for a mass flow rate of 0.02 kg s^{-1} , the corresponding values obtained were $8.5 \text{ W m}^{-2} \text{ K}^{-1}$ and $8.67 \text{ W m}^{-2} \text{ K}^{-1}$, respectively. Hence, it was concluded that channel depth was a significant parameter, which influences the convective heat transfer within the DPSAHS. The convection losses from the glass cover to the ambient environment was also

estimated using McAdams correlation [19]. As the McAdams correlation depends only on the value of wind velocity, the convection loss from the glass cover was found to be almost constant for both the mass flow rates based on which the thermodynamic analysis was carried out.

Instantaneous Efficiency (η)

The instantaneous efficiency of the described DPSAHS is a function of the amount of heat gained and the incident solar radiation over the collector area. As mentioned in Eq. (40), the instantaneous efficiency of the system varies inversely with respect to the incident solar radiation over the collector surface. Hence, as the solar radiation reduces, the instantaneous efficiency tends to rise abruptly at that particular instance and vice versa. These fluctuations were easily identifiable from the sudden peaks and are shown in Fig. 7. At every instance, even though the solar intensity value may drop down due to sudden changes in meteorological conditions (such as cloud cover) the air temperature does not drop rigorously. It was due to the inherent thermal inertia characteristics of each individual component present within the DPSAHS. The stored energy given away by these surfaces balances the sudden drop in solar intensity for a shorter time. However, if the solar intensity tends to drop continuously, the air temperature decreases (as the temperature of enclosing surfaces reduces). At a mass flow rate corresponding to 0.02 kg s^{-1} , the values of instantaneous efficiency ranges from 0.034% (8:00 am) to 32.07%

(17:00 pm) with a peak value of 149.6% (15:30 pm). Similarly at 0.03 kg s^{-1} , the instantaneous efficiency values ranges from 7.46% (8:00 am) to 58.82% (17:00 pm) with a peak value of 302.98% (15:30 pm). All the peak values correspond to that particular instant of time when the solar intensity dropped to a lower value. It was caused due to unexpected change in climatic conditions. In addition, it was concluded that, due to the estimation of instantaneous efficiency by Eq. (40), a clear demarcation on the performance of the described DPSAHS cannot be obtained.

Overall efficiency (η_I)

Based on the comparison made with respect to the variation of solar intensity and mass flow rate, it was identified that the instantaneous efficiency was not a benchmark tool to evaluate the thermodynamic performance of the described system. Hence, the formula to compute the daily overall thermal efficiency of the system is modified as mentioned in Eq. (41). To account for the sudden changes in solar intensity and to address the sensible heat content of the enclosed surfaces, an integral formulation was adopted. The present analysis showed that the daily overall thermal efficiency of the system corresponding to a mass flow rate of 0.02 kg s^{-1} varied from 21.1% (9:00 am) to 36.7% (17:00 pm). Similarly, corresponding to 0.03 kg s^{-1} the overall thermal efficiency varied from 27% (9:00 am) to 41% (17:00 pm), respectively. The obtained results inferred that, as the mass flow rate increases, the heat gained by

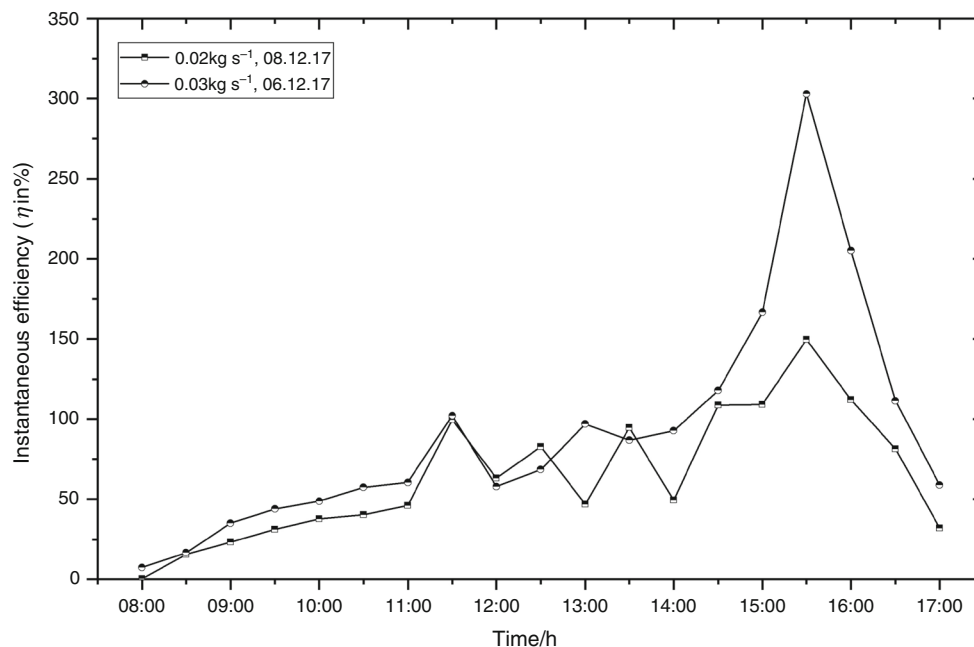


Fig. 7 Instantaneous efficiency variation corresponding to two different mass flow rates

the air from the enclosed channel passages increases. As a result, the daily overall thermal efficiency increases with respect to the incident solar radiation and vice versa. Figure 8 shows the comparison of daily overall thermal efficiency variation corresponding to two different mass flow rates as described.

Based on Fig. 8, it was observed that there was an increasing trend in the overall thermal efficiency variation from 9:00 am to 17:00 pm. The trend thus observed was mainly due to the sensible heat storage capacity of the enclosed surfaces within the DPSAHS. As mentioned in Sect. 5.5, the enclosed surfaces tend to give away the stored heat whenever the solar intensity drops at any instance. On the other hand, from the beginning to the peak sunshine hours, the amount of energy stored in the absorber and the bottom plate (considering them as major contributors) tends to rise, even though a part of it was convected away by the air flowing through the channel passages. Similarly, when the solar intensity tends to decrease (from 15:00 pm), the enclosed surfaces still absorb and store the available amount of energy (a part of it is still convected out by air). However, the energy extracted out by the air may not be as high in magnitude as it was corresponding to the peak solar insolation hours. Thus, it was concluded that, even though the solar insolation drops off in its value, the sensible heat content of the enclosed surfaces give away the stored heat to the air mass. If the experiments were further continued beyond 17:00 pm, the overall efficiency would start decreasing as there was lack of sufficient heat (solar insolation drops below 100 W m^{-2} and tends to zero) to be absorbed by the enclosing surfaces, as its stored energy was already drained by the air flowing

through the channel passages. This effect has contributed to the rise in the overall thermal efficiency trend as shown in Fig. 8. In addition, the results obtained from the present analysis were compared with the experimental findings (thermal efficiency variation of single-pass solar air heater) of Chabane et al. [26] as shown in Fig. 8. The results of Chabane et al. [26] correspond to a mass flow rate of 0.02 kg s^{-1} . Their results were found to have a similar trend with respect to the present experimental findings. The observed variations (rise and fall) in the results of Chabane et al. [26] are possibly due to the uncertainties associated with the meteorological conditions of that specific location.

Exergy Efficiency (η_{II})

Exergy analysis was performed based on the recorded experimental data and by using equations mentioned in Sect. 4.2. For simplicity of calculations, the sun temperature was considered to be a constant value of 6000 K [26]. The analysis was performed corresponding to two different mass flow rates of 0.02 kg/s and 0.03 kg s^{-1} , respectively. The exergy efficiency was found to vary from 5.6% (9:00 am) to 13.2% (17:00 pm) corresponding to a mass flow rate of 0.02 kg s^{-1} . Similar trend was observed in the exergy efficiency variation corresponding to flow rate of 0.03 kg s^{-1} . The values were found to be in the range of 8.5% (9:00 am) to 18.04% (17:00 pm). Figure 9 shows the variation of exergy efficiency of the DPSAHS at various time intervals corresponding to two different mass flow rates. From the plot, it was inferred that, as the mass flow rate increases, the exergy efficiency also increases. As

Fig. 8 Overall thermal efficiency variation corresponding to two different mass flow rates

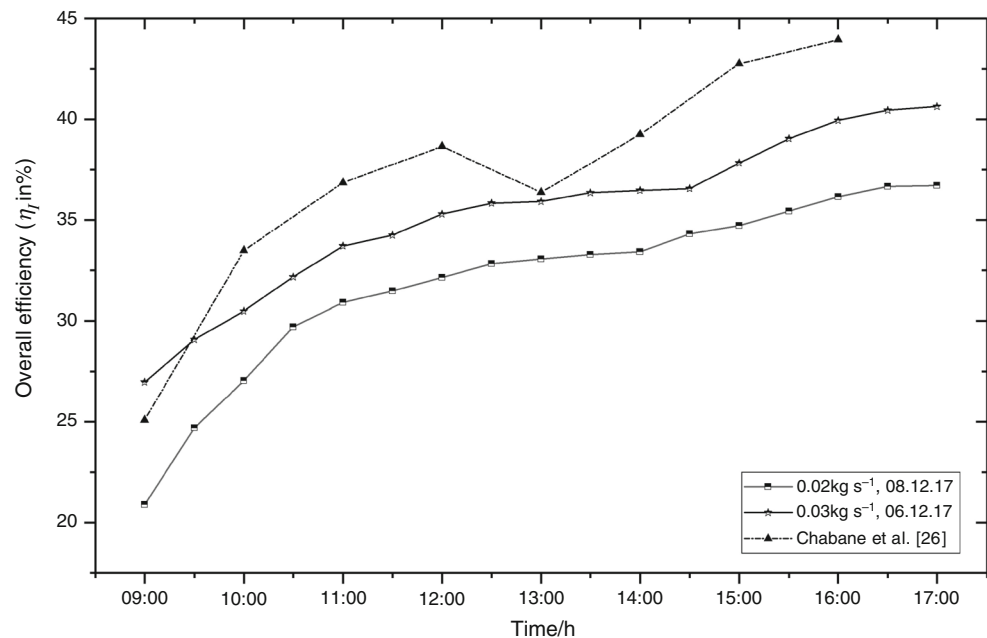
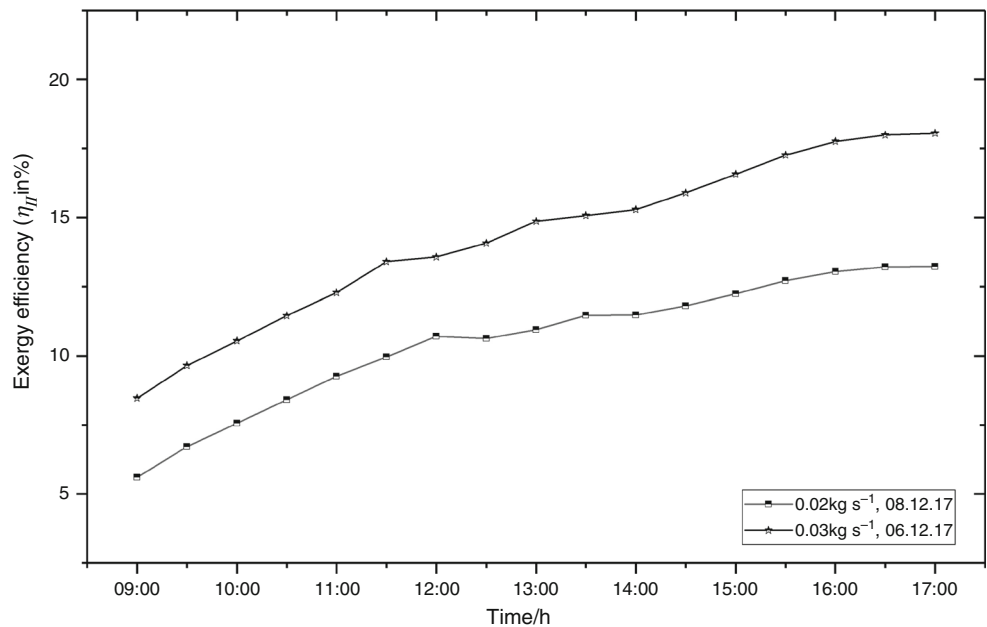


Fig. 9 Exergy efficiency corresponding to two different mass flow rates



mentioned in Sect. 5.6, the overall thermal efficiency of the DPSAHS increases with increase in mass flow rate. Hence, the amount of useful energy, which can be extracted from the overall system, was higher at higher flow rate. Thereby, the exergy efficiency increases along with an increase in mass flow rate through the air heater system. In addition, the exergy efficiency accounts only about 18% corresponding to 0.03 kg s^{-1} , even though the overall thermal efficiency obtained was 41%. It was due to the provision of double-pass flow configuration, which has led to an increase in heat losses from the DPSAHS. In addition, the obtained experimental findings were found to be in good agreement with the reported works of Esen [18], Alta et al. [28] and Languri et al. [29].

It is to be noted that the thermophysical property variation, especially the specific heat capacity of the working fluid (air), remains a constant throughout, within the operating temperature regime of $20\text{--}70 \text{ }^\circ\text{C}$. Density, thermal conductivity, and viscosity of the working fluid were found to have a net variation of 4.07%, 4.6%, and 3.52%, respectively. Thus, the stated expressions used for computing the daily overall thermal efficiency helped to reduce the sudden fluctuations in the results, which were earlier caused due to the inherent intermittency of solar radiation. Thereby, a more realistic quantification for the overall thermal performance of the described DPSAHS was obtained.

Pressure drop

Pressure drop calculations were carried out based on the mentioned Eqs. (36)–(39) in Sect. 4.1. The total pressure

drop across the solar air heater system comprises of pressure drops occurring at the inlet and exit section along with the pressure variation occurring within the channel passages. At mass flow rates of 0.02 kg s^{-1} and 0.03 kg s^{-1} , the variation in pressure drop was calculated. The results confirmed that the pressure drop within the air heater system increases as the flow velocity through the channel passages increases. In addition, due to the flow reversal occurring between the upper and lower channel passages, there is a significant rise in pressure drop in the double-pass arrangement. The range of values for pressure drop obtained corresponding to two different mass flow rates of 0.02 kg s^{-1} and 0.03 kg s^{-1} were $0.13\text{--}0.47 \text{ N m}^{-2}$, respectively. The obtained results were found to be in good agreement with the experimental works reported by Kumar et al. [30]. Based on their experimental investigation on a conventional single-pass flat plate configuration, the obtained values of pressure drop was in the range of $0.06\text{--}0.26 \text{ N m}^{-2}$. However, for the present experimental investigation, the obtained values were found to be higher. This was mainly due to the flow reversal occurring within the channel passages of the DPSAHS.

Parametric analysis of DPSAHS

A prediction model was initially developed using ANN toolbox in order to perform the parametric analysis. A feed-forward back propagation (FFBP) algorithm with 4-25-4 configuration was found to predict the performance characteristics of the DPSAHS satisfactorily. In the present analysis, LM training function with 25 hidden neurons and Log-Sigmoidal as the activation function predicted the

thermal efficiency and exergy efficiency of the experimental setup with least error. The maximum value of R^2 and minimum values of RMSE and COV obtained were 0.99993, 0.00621, and 0.0177, corresponding to flow rate of 0.02 kg s^{-1} . Similarly, at 0.03 kg s^{-1} , the obtained values of maximum R^2 and minimum values of RMSE and COV were 0.99995, 0.00467, and 0.0151, respectively. In the present analysis, ANOVA technique was used to identify the major ambient parameters affecting the thermal performance of the DPSAHS [17]. Table 5 demonstrates the overall percentage contribution of parameters such as solar intensity, ambient temperature, wind speed, and relative humidity on the overall thermal efficiency and exergy efficiency of the test facility.

Influence of solar intensity

Solar intensity incident on to the absorber surface (transmitted by the glass cover) acts as the major source of thermal energy for the air flowing through the collector passages. During the peak sunshine hours, the energy gained by the absorber surface increases which in turn improves the heat gained by the air flowing over the absorber surface. Thus, the amount of useful heat extracted from the DPSAHS improves with increase in solar intensity and vice versa. At the same time, the radiative losses from the absorber, bottom plate, and glass cover increases with increase in magnitude of incident solar radiation. Based on ANOVA analysis, it was found that solar intensity accounts for 44.5% (percentage contribution) of the variation in overall thermal efficiency of the DPSAHS during its operation. Similarly, a major contributor towards the exergy efficiency variation was solar intensity and it accounts to 50.1% of the total percentage contribution.

Influence of ambient temperature

Air flowing through the collector gains thermal energy due to the temperature gradient existing between the enclosed components within the DPSAHS and the ambient air. In general, during the peak sunshine hours, the ambient temperature tends to rise. However, the variation in ambient temperature was found to be less than 2°C corresponding to these peak hours. It was observed that higher the temperature gradient, higher would be the heat gained by the air. Based on ANOVA analysis, ambient temperature was found to be the major contributor towards the overall thermal efficiency variation and accounts to 49.1% of the total contribution. For the variation in exergy efficiency of the DPSAHS, ambient temperature accounts for 40.6% of the total percentage contribution.

Influence of wind speed and other parameters

Wind speed was found to contribute to 4.1% and 6.2% of the total percentage contribution towards the overall thermal efficiency and exergy efficiency variation of the DPSAHS. Convective heat loss from the glass cover is a strong function of wind speed. Higher the wind speed, the glass cover temperature will reduce and will lead to an increase in heat losses due to build of a temperature gradient. In comparison with solar intensity and ambient temperature, the effect of wind speed on the thermal performance characteristics of DPSAHS is comparatively less, but cannot be neglected. Relative humidity is yet another factor that may influence the performance of the system. Among the four parameters considered for the ANOVA analysis, relative humidity was found to be the least contributor towards both overall thermal efficiency and exergy efficiency variation and it accounts for 2.3% and 3.1%, respectively. When the amount of moisture present in air is high, the moisture may condense and wet the surface of the glass cover. This may influence the transmission of incident solar radiation from the glass cover to the absorber surface. Similarly, the deposition of dust particles present in the atmosphere over the glass surface may also reduce the thermal performance of the DPSAHS. Hence, it is necessary to clean the surface of glass cover regularly with a soft cloth or water before starting the operation. Though, relative humidity and dirt accumulation may seem to have a little influence on the thermal performance of the DPSAHS in comparison with other parameters, in the long run, their effect on the overall performance cannot be neglected.

Possible performance improvements

In general, based on the exergy analysis carried out at different mass flow rates, it was concluded that the mass flow rate was a significant parameter, which affects the overall thermal performance of the DPSAHS. Hence, the exergy destruction within the DPSAHS can be reduced by controlling the airflow rate. An air blower provided with a variable frequency controller is highly recommended which would help to provide a more accurate control over the system performance rather than that of using gate valves. A leak-proof design is yet another criterion, which would improve the overall energy as well as reduce the exergy destruction within the DPSAHS. Therefore, it is advisable to provide gas-welded joints at sharp corners and bends. The exergy loss through the glass cover could be minimized by the provision of double-glazing covers at the top surface. This would help to minimize the convection losses from the glass cover as well as the radiative losses from the absorber surface.

Conclusions

A conventional energy and exergy analysis is carried out to investigate the thermal performance characteristics of a DPSAHS provided with asymmetric channel passages. The following conclusions drawn based on the present experimentation are:

- a. Energy and exergy performance characteristics of the DPSAHS are found to be a strong function of mass flow rate, channel depth, and ambient parameters.
- b. Parametric analysis concludes that solar intensity and ambient temperature are significant parameters, which affect the thermodynamic behaviour of the DPSAHS followed by wind speed.
- c. Relative humidity variation shows a relatively smaller percentage contribution towards energy and exergy performance characteristics of DPSAHS.
- d. Overall thermal efficiency varies in the range of 20–41% corresponding to flow rates of 0.02 kg s^{-1} and 0.03 kg s^{-1} , respectively.
- e. Exergy efficiency of DPSAHS varies between the ranges of 5.6–18.04% with mass flow rate. Lower exergy efficiency is attributed to the increase in losses occurring due to the provision of double-pass configuration.
- f. The effect of thermophysical properties on the performance is found to be dependent on the operating temperature as well as the nature of working fluid used.
- g. Pressure drop across the DPSAHS is found to increase with increase in mass flow rate within the range of $0.13\text{--}0.47 \text{ N m}^{-2}$.

References

1. Suzuki A. General theory of exergy-balance analysis and application to solar collectors. *Energy*. 1988;13(2):153–60. [https://doi.org/10.1016/0360-5442\(88\)90040-0](https://doi.org/10.1016/0360-5442(88)90040-0).
2. Ajam H, Farahat S, Sarhaddi F. Exergetic optimization of solar air heaters and comparison with energy analysis. *Int J Thermodyn*. 2005;8(4):183–90.
3. Hernández AL, Quiñonez JE. Analytical models of thermal performance of solar air heaters of double-parallel flow and double-pass counter flow. *Renew Energy*. 2013;55:380–91. <https://doi.org/10.1016/j.renene.2012.12.050>.
4. Velmurugan P, Kalaivanan R. Energy and exergy analysis of multi-pass flat plate solar air heater—an analytical approach. *Int J Green Energy*. 2015;12(8):810–20. <https://doi.org/10.1080/15435075.2014.888662>.
5. Hollands KGT, Shewen EC. Optimization of flow passage geometry for air-heating, plate-type solar collectors. *J SolEnergy Eng*. 1981;103(4):323–30. <https://doi.org/10.1115/1.3266260>.
6. Verma R, Chandra R, Garg HP. Optimization of solar air heaters of different designs. *Renew Energy*. 1992;2(4–5):521–31. [https://doi.org/10.1016/0960-1481\(92\)90091-G](https://doi.org/10.1016/0960-1481(92)90091-G).
7. Mortazavi A, Ameri M. Conventional and advanced exergy analysis of solar flat plate air collectors. *Energy*. 2018;142:277–88. <https://doi.org/10.1016/j.energy.2017.10.035>.
8. Gupta MK, Kaushik SC. Exergetic performance evaluation and parametric studies of solar air heater. *Energy*. 2008;33(11):1691–702. <https://doi.org/10.1016/j.energy.2008.05.010>.
9. Hegazy AA. Performance of flat plate solar air heaters with optimum channel geometry for constant/variable flow operation. *Energy Convers Manag*. 2000;41(4):401–17. [https://doi.org/10.1016/S0196-8904\(99\)00052-7](https://doi.org/10.1016/S0196-8904(99)00052-7).
10. Sun W, Ji J, He W. Influence of channel depth on the performance of solar air heaters. *Energy*. 2010;35(10):4201–7. <https://doi.org/10.1016/j.energy.2010.07.006>.
11. Kalogirou SA, Karellas S, Badescu V, Braimakis K. Exergy analysis on solar thermal systems: a better understanding of their sustainability. *Renew Energy*. 2016;85:1328–33. <https://doi.org/10.1016/j.renene.2015.05.037>.
12. Benli H. Experimentally derived efficiency and exergy analysis of a new solar air heater having different surface shapes. *Renew Energy*. 2013;50:58–67. <https://doi.org/10.1016/j.renene.2012.06.022>.
13. Handbook, A.S.H.R.A.E. American Society of Heating, Refrigeration and Air-Conditioning Engineers, Inc. 2001.
14. Esen H, Ozgen F, Esen M, Sengur A. Artificial neural network and wavelet neural network approaches for modelling of a solar air heater. *Expert Syst Appl*. 2009;36(8):11240–8. <https://doi.org/10.1016/j.eswa.2009.02.073>.
15. Benli H. Determination of thermal performance calculation of two different types solar air collectors with the use of artificial neural networks. *Int J Heat Mass Transf*. 2013;60:1–7. <https://doi.org/10.1016/j.ijheatmasstransfer.2012.12.042>.
16. Islamoglu Y, Kurt A. Heat transfer analysis using ANNs with experimental data for air flowing in corrugated channels. *Int J Heat Mass Transf*. 2004;47(6–7):1361–5. <https://doi.org/10.1016/j.ijheatmasstransfer.2003.07.031>.
17. Gunasekar N, Mohanraj M, Velmurugan V. Artificial neural network modeling of a photovoltaic-thermal evaporator of solar assisted heat pumps. *Energy*. 2015;93:908–22. <https://doi.org/10.1016/j.energy.2015.09.078>.
18. Esen H. Experimental energy and exergy analysis of a double-flow solar air heater having different obstacles on absorber plates. *Build Environ*. 2008;43(6):1046–54. <https://doi.org/10.1016/j.buildenv.2007.02.016>.
19. McAdams WH. Heat transmission. 3rd ed. New York: McGraw Hill; 1954.
20. Duffie JA, Beckman WA. Solar engineering of thermal processes. New York: Wiley; 1982.
21. Bahrehmand D, Ameri M. Energy and exergy analysis of different solar air collector systems with natural convection. *Renew Energy*. 2015;74:357–68. <https://doi.org/10.1016/j.renene.2014.08.028>.
22. Dincer I. Thermodynamics, exergy and environmental impact. *Energy Sources*. 2000;22(8):723–32. <https://doi.org/10.1080/00908310050120272>.
23. Karsli S. Performance analysis of new-design solar air collectors for drying applications. *Renew Energy*. 2007;32(10):1645–60. <https://doi.org/10.1016/j.renene.2006.08.005>.
24. Altfeld K, Leiner W, Fiebig M. Second law optimization of flat-plate solar air heaters. Part I: the concept of net exergy flow and the modeling of solar air heaters. *Sol Energy*. 1988;41(2):127–32. [https://doi.org/10.1016/0038-092X\(88\)90128-4](https://doi.org/10.1016/0038-092X(88)90128-4).
25. Kumar RA, Babu BG, Mohanraj M. Thermodynamic performance of forced convection solar air heaters using pin-fin absorber plate packed with latent heat storage materials. *J Therm*

- Anal Calorim. 2016;126(3):1657–78. <https://doi.org/10.1007/s10973-016-5665-6>.
26. Chabane F, Moumni N, Benramache S. Experimental study of heat transfer and thermal performance with longitudinal fins of solar air heater. *J Adv Res.* 2014;5(2):183–92. <https://doi.org/10.1016/j.jare.2013.03.001>.
27. Forson FK, Nazha MA, Rajakaruna H. Experimental and simulation studies on a single pass, double duct solar air heater. *Energy Convers Manag.* 2003;44(8):1209–27. [https://doi.org/10.1016/S0196-8904\(02\)00139-5](https://doi.org/10.1016/S0196-8904(02)00139-5).
28. Alta D, Bilgili E, Ertekin C, Yaldiz O. Experimental investigation of three different solar air heaters: energy and exergy analyses. *Appl Energy.* 2010;87(10):2953–73. <https://doi.org/10.1016/j.apenergy.2010.04.016>.
29. Languri EM, Taherian H, Hooman K, Reisel J. Enhanced double-pass solar air heater with and without porous medium. *Int J Green Energy.* 2011;8(6):643–54. <https://doi.org/10.1080/15435075.2011.600379>.
30. Kumar RA, Babu BG, Mohanraj M. Experimental investigations on a forced convection solar air heater using packed bed absorber plates with phase change materials. *Int J Green Energy.* 2017;14(15):1238–55. <https://doi.org/10.1080/15435075.2017.1330753>.